Spectrochimica Acta Part A: Molecular and Biomolecular Spectroscopy 104 (2013) 505–511

Contents lists available at SciVerse ScienceDirect

Spectrochimica Acta Part A: Molecular and Biomolecular Spectroscopy

journal homepage: www.elsevier.com/locate/saa

Crystal field effect on EPR and optical absorption properties of natural green zoisite

Henry Javier-Ccallata *, Shigueo Watanabe

Departamento de Física Nuclear, Instituto de Física, Universidade de São Paulo, Rua do Matão, Travessa R, 187, CEP 05508-900, São Paulo, SP, Brazil

HIGHLIGHTS

- The crystal structure of zoisite does not change for high temperature annealing between 500 and 900 °C.
- The simultaneous appearance of EPR lines, at $g = 6$ and 4, is uncommon making our result interesting.
- Deconvolution analysis shows 8 EPR absorption bands which were attributed to Cr^{3+} and Fe^{3+} ions.

GRAPHICAL ABSTRACT

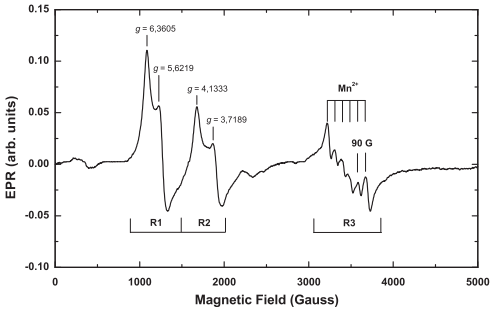

ARTICLE INFO

Article history:
Received 24 September 2012
Received in revised form 25 November 2012
Accepted 27 November 2012
Available online 13 December 2012

Keywords:
Zoisite
Optical absorption
Annealing
EPR
Crystal field

ABSTRACT

In this study the electron paramagnetic resonance (EPR) and optical absorption (OA) of natural crystal of zoisite were investigated after γ (^{60}Co) irradiation and high temperature annealing. EPR measurements show that the zoisite from Tefilo Otoni MG Brazil contain Cr^{3+}, Fe^{3+} and Mn^{2+} ions and occupy distorted Al^{3+} octahedral and tetrahedral sites which are subjected to the action of a strong crystal field in axial direction. Absorption bands which in principle give rise to sets of EPR lines between 500 and 2500 G were found using the deconvolution method. The application of high doses of gamma ray and high temperature annealing has shown no significant effects on EPR and OA spectra. Spin-allowed, spin-forbidden and crystal field parameters were calculated for $3d^3$ configuration and interpreted using the spin Hamiltonian formalism containing axial and rhombic terms in low symmetries.

Introduction

Zoisite is a sorosilicate, one of the members of the epidote group, and like other mineral members of this group, is characterized by the presence of double tetrahedron (Si_2O_7) that links to the octahedral chains forming orthorhombic structures [1–7]. The presence of Fe^{3+}, Cr^{3+}, Mn^{2+} and $V^{2+/3+}$ ions replacing Al^{3+} in the ideal formula, $Ca_2Al_3(SiO_4)$ (Si_2O_7) O (OH), causes changes in the local symmetry of the octahedra and tetrahedra in the crystal such that it acquires very interesting optical and luminescent properties that have been studied by several authors [3,8–23]. Zoisite samples synthesized with its main components have a weak blue–green color [18]. However, with the inclusion of transition metal ions a zoisite acquires several colors. Zoisite becomes pink colored with the inclusion of small concentrations of Mn^{2+} ions and is called thulite [21]. Excess of $V^{2+/3+}$ and Fe^{3+} ions turns zoisite to blue and is known as tanzanite and has a high commercial value [6,24–26]. With the inclusion of chromium ions, zoisite acquires an intense green color and can be used in jewelry and ornaments [27].

Electron paramagnetic resonance (EPR) studies by Tsang and Ghose [23] attributed the line at low magnetic field ($g \sim 6$) to Fe^{3+} ion in position II of the octahedron. On the other hand, Hutton et al. [13] considered the same EPR line, at low magnetic field, as being due to transitions of Cr^{3+} ion. Transitions due to Cr^{3+} ion in the octahedral site make the g-factor changes from 2 to 4, this is due to a transition from $-\frac{1}{2}$ to $+\frac{1}{2}$ in a doublet $|\pm\frac{1}{2}>$ of a spin

* Corresponding author. Address: Av. Independencia s/n, Universidad Nacional de San Agustín, Arequipa, Peru. Tel.: +51 974367388.
E-mail address: henrysjc@gmail.com (H. Javier-Ccallata).

1386-1425/$ - see front matter © 2012 Elsevier B.V. All rights reserved.
http://dx.doi.org/10.1016/j.saa.2012.11.099

system $S = 3/2$. This transition may be due to a very strong crystal field in an octahedral environment of low symmetry. Following this reasoning Czaja et al. [10] studied the effect of the crystal field on V^{3+} and Cr^{3+} ions in tanzanite and attributed the blue color to the $^4A_2 \rightarrow {}^4T_2$ transition in the large non-cubic crystal field.

In the studies of the optical absorption (OA), Schmetzer and Berdesinski [27] attributed the bands at 662 and 458 nm to the Cr^{3+} in an octahedral environment. Koziarska et al. [14] studied the tanzanite with high concentration of $V^{2+/3+}$ and Cr^{3+} ions and indicated that Cr^{3+} ion as responsible for the intense luminescence in tanzanite. Additionally it was shown and suggested that due to ample luminescent spectrum in the infra-red region, zoisite can be an interesting material for laser applications.

In recently published works Ccallata et al. [9] and Ccallata and Watanabe [28] found that zoisite from Tefilo Otoni MG, Brazil, has uncommon thermoluminescence (TL) sensitivity after high temperatures pre-annealing. It was found that a maximum TL emission can be obtained when a sample is pre-annealed at 600 °C. The TL mechanism proposed takes into account Al^{3+}, Ti^{3+} and E_1' centers.

In this paper, EPR and OA properties of zoisite annealed at high temperatures have been investigated.

The crystal field parameters (Dq, Δ and B) were determined and used to analyze the energy levels in the ground state of zoisite. Using the spin Hamiltonian formalism can be explained both shape and position of EPR lines.

Experimental

All measurements were performed on samples of zoisite obtained at Tefilo Otoni in the state of Minas Gerais-Brazil. The crystal is characterized by an intense green color. Enough portion of the zoisite was ground into powders keeping grains of the size between 0.080 and 0.180 mm to be used for EPR and TL measurements. Grains smaller than 0.080 mm were used in the X-ray fluorescence and X-ray diffraction analysis. For the OA experiments five slabs with 1.0 ± 0.1 mm thickness were cut and well polished.

The chemical composition of the sample has been determined by X-ray fluorescence analysis using a Phillips PW2404 spectrometer at the Laboratory of Technological Characterization of the Polytechnic School. To certify that the sample to be investigated is actually a zoisite, X-ray diffraction analysis was carried out using MiniFlex II diffractometer in natural sample and samples annealed at 500, 600, 700 and 800 °C. The EPR measurements have been carried out using Bruker EMX spectrometer with a rectangular cavity ER4102ST with a microwave frequency of 9.767 GHz (X-band). Optical spectra were obtained utilizing a Varian Cary Model 500 UV–Vis–NIR spectrometer. All γ-ray irradiations have been carried out at IPEN Institute for Energy and Nuclear Research using a ^{60}Co source with a dose rate of 4.70 ± 0.09 kGy h^{-1} at room temperature.

Results

Fig. 1 shows the diffraction patterns of natural zoisite and samples that had been annealed at 500, 600, 700, 800 and 900 °C. The patterns are compared with the powder diffraction file (PDF) No. 13-0562 of synthesized zoisite. The lines that characterize the crystalline phase of zoisite, labeled in Fig. 1, remain in the same positions indicating that the crystal does not change phase at high temperature annealing. Note that the line at 511 shows high intensity after 800 °C annealing and decreases after annealing at 900 °C. On the other hand, the line 312 and their satellites, show a small change in the intensity after 600 and 800 °C annealing. However despite these small variations in intensity, 90% of lines remain in

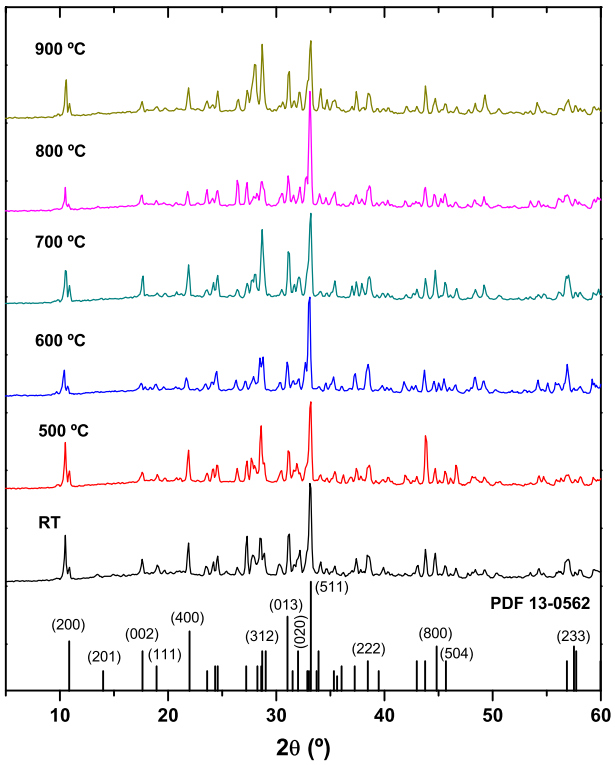

Fig. 1. Comparison of the powder diffraction file No. 13-0562 of orthorhombic zoisite with X-ray diffraction data of zoisite samples without heat treatment and with annealing at 500, 600, 700, 800 and 900 °C.

Table 1
Chemical analysis of zoisite by X-ray fluorescence. The main oxides of natural sample are shown in the second column and the oxides in smaller quantities in the last column.

Oxides	mol%	Oxides	mol%
SiO_2	40.2	K_2O	0.28
Al_2O_3	23.2	SrO	0.19
CaO	25.1	TiO_2	0.14
Fe_2O_3	2.87	BaO	0.13
MgO	2.55	MnO	0.06
Cr_2O_3	1.21	P_2O_5	0.03
NaO	0.90	SO_3	0.02
		ZnO	0.02
		NiO	0.02

the 2θ-positions described by the PDF pattern. Other less intense lines due to impurities are observed and these lines show slight differences in intensity from one annealing to the another. This result confirms that the crystal structure of zoisite mineral do not change with high temperature annealing.

Table 1 shows in the first column besides the main oxides constituents (SiO_2, Al_2O_3 and CaO), the main impurity oxides, i.e. Fe $_2O_3$, MgO, Cr_2O_3 and NaO. In the second column other impurity oxides are shown which are in smaller concentrations. According to Game [29] the amount of oxides in a sample of zoisite without impurities is approximately SiO_2 (39.67%), Al_2O_3 (33.66%), and CaO (24.68%). This result compared with ours (Table 1) indicates a deficiency of Al_2O_3 by 10.46 mol%. This deficit of Al^{3+} in the structure can be covered by other oxides such as Fe_2O_3 (Fe^{3+}), Cr_2O_3 (Cr^{3+}) and TiO_2 (Ti^{3+}).

Fig. 2 shows the EPR spectrum for a sample of zoisite at room temperature. The spectrum shows three sets of lines, R1 (800–1500 G), R2 (1500–2000 G) and R3 (3100–3900 G). The simultaneous appear-

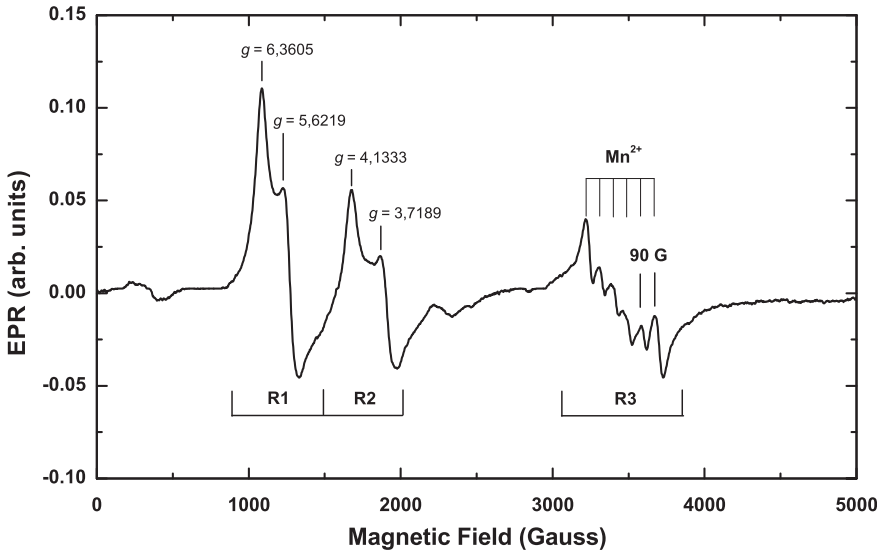

Fig. 2. EPR spectrum of natural zoisite. Measurements performed with microwave frequency of 9.77 GHz and microwave power of 20.2 MW at room temperature on a Bruker X-band spectrometer.

ance of two sets of lines, R1 and R2, is not mentioned in the literature making our result particularly interesting. In the EPR studies carried out by Tsang and Ghose [23] with tanzanite, they attributed the isotropic line at low magnetic field ($g \sim 4.3$) to the Fe^{3+} that substitutes the Al^{3+} in the position II of the octahedral site. However Hutton [12] attributed this line to Cr^{3+} ion. In the R3 set can be identified the six intense hyperfine lines of the Mn^{2+} with typical values of g around 2.028(2) and A = 90(1), note that in the spectrum do not exist hyperfine interaction lines such as in other sorosilicate minerals. A similar study by Srinivasulu et al. [21] with zoisite mineral rich in Mn^{2+} (Thulite), indicate the same lines due to Mn^{2+} superimposed to the intense spin–spin interaction due to Fe^{3+} ion around g = 2. The experimental values of g and A are in agreement with those of Mn^{2+} in epidote minerals [23].

The EPR spectrum of samples pre-annealed at high temperatures and then irradiated to 50 kGy of gamma-ray is shown in Fig. 3. The pre-annealing up to 600 °C seems to introduce very small change, but the intensity of lines in R1 and R2 regions decrease for annealing at 900 °C and for the R3 region, six lines of Mn^{2+} becomes wider. Notice also the small signal centered at g = 2.010 that increase with the gamma dose, possibly due to the peroxy center (OHC) that appear by inclusion of oxygen vacancy in SiO_4 tetrahedrons in the structure [30].

The optical absorption spectrum of zoisite (Fig. 4) shows several absorption bands in different regions. In the near ultraviolet region, a band around 385 nm was identified. In the visible region one band at 427 nm due to aluminum center and three intense bands at 453, 658 and 691 nm due to allowed transitions of Cr^{3+} in octahedral positions of structure are observed.

The shape of the broad band between 550 and 750 nm suggest that transitions due to other ions are covered by the intense band of Cr^{3+} (inset of Fig. 4). Additionally the sharp drop at ~680 nm indicates the effect of a strong crystal field in the axial direction of the octahedral site that contain the Cr^{3+} ion.

Several absorption bands appear in the near infrared (NIR) region. A broad band centered at 1400 nm (7143 cm^{-1}) was attributed to the first and second longitudinal vibration modes of OH^- ion. Similarly intense bands at 1666 nm (6000 cm^{-1}) and 2300 nm (4347 cm^{-1}) were identified as vibration modes of OH ion. The remaining bands in Fig. 4, i.e. 1847 nm (5414 cm^{-1}), 1935 nm (5168 cm^{-1}) and 2474 (4042 cm^{-1}), were attributed to

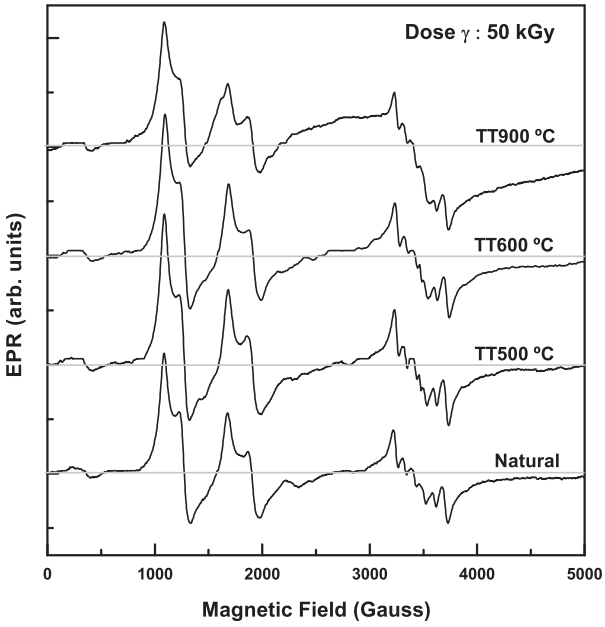

Fig. 3. EPR spectra of natural and thermally annealed zoisite at 500, 600 and 900 °C which have been subsequently irradiated with 50 kGy of gamma dose.

water molecules in the crystal structure. OA studies by Hunt et al. [31] with several natural silicate minerals have been attributed to the hydroxyl ions related to Fe^{3+}, Al^{3+}, Mn^{2+} and Cr^{3+} (*metal*–O–H) that produce vibrational modes at 2200 and 2300 nm. It is interesting to note that the Fe^{2+} band is absent; in many other silicate minerals it usually appears.

Optical absorption spectra of zoisite annealed at 500, 600, 700 and 800 °C are shown in visible and infrared regions of the spectrum in Fig. 5a and b. No changes are observed in the bands except for an increase in the background of spectrum. The strong crystal field effect is identified by the sharp drop at 680 nm. The vibrational modes of OH and H_2O ions do not change (Fig. 5b). The strong increase in the background absorption is usually accompanied by the fact that the crystal becomes darker as the annealing temperature increases.

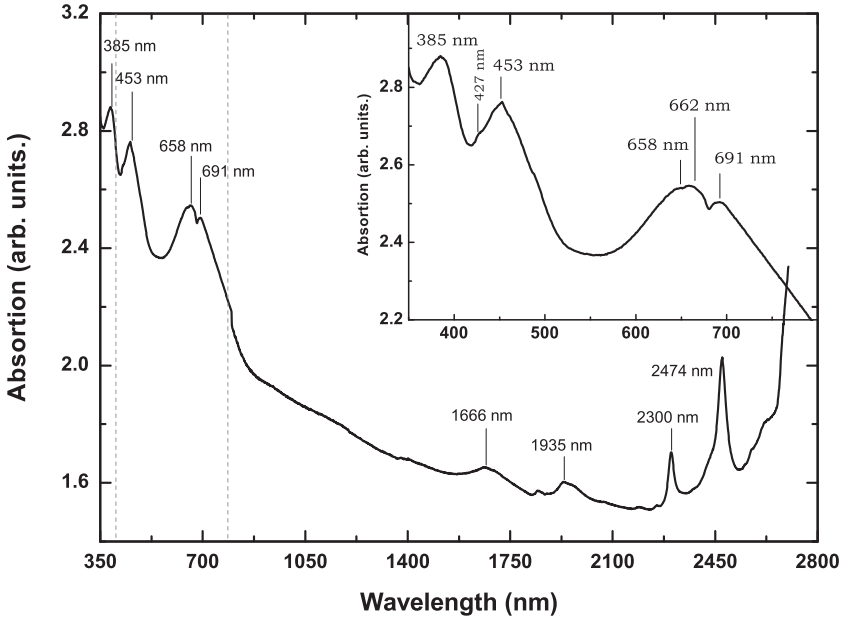

Fig. 4. Optical absorption bands of zoisite in UV, Vis and IR regions. The inset shows details of the spectrum in the visible region.

Discussion

Crystal structure

For the discussion of both optical absorption and EPR spectra, let us consider the structure of the zoisite crystal. According to Dollase [2] the structure contains chains, parallel to *y*, of edge-sharing octahedra of two kinds: one is the edge sharing (M2) and the other a chain of two octahedra (M1) and (M3) attached on alternated sides along its lengths. M1 and M2 are cations sites that are centrosymmetric, whereas M3 is non-centrosymmetric. A single tetrahedra (SiO_4) bridge the chains of octahedra in the *z*-axis direction and double tetrahedra (Si_2O_7) do the same. The framework formed this way create relatively large cavities (*A*) occupied by Ca ions in nine or ten-fold coordination. The M2 octahedra containing only Al ions, M3 contains non-Al ions, such as Fe^{3+} and Mn. The M2 site is coordinated by hydroxyl OH.

The energy diagram of Cr^{3+} in an octahedral crystal field

Fig. 6 shows Tanabe–Sugano energy level diagram for Cr^{3+}: $3d^3(^4F)$ in octahedral coordination.

While 453, 458 and 691 nm bands seem to be attributable to Cr^{3+} ion in an octahedral site, the 427 nm band is due to [AlO_4/*h*]-center. Studies by Fuxi and Huimin [32], indicate that broad bands are due to allowed transitions of Cr^{3+} ion in a distorted octahedron in the axial direction. This strong distortion appears in M3 octahedron in zoisite and other epidote minerals. Our results suggest that the broad band centered at 662 nm is broken giving two bands with maximum around 658 nm and 691 nm. On the other hand it is well known that in quartz and the many crystals of silicate Al^{3+} replaces frequently SiO_4 in (SiO_4) ending in [AlO_4/*h*]-center.

Schmetzer and Berdesinski [27] attributed 15100 cm^{-1} and 21800 cm^{-1} bands as due to transitions v_1, $^4A_2 \rightarrow {}^4T_2$) and ($v_2$, $^4A_2 \rightarrow {}^4T_1$) respectively in zoisite. The Racah parameter *B* is defined as:

$$B = \frac{(2v_1 - v_2)(v_2 - v_1)}{27v_1 - 15v_2} \quad (1)$$

therefore, they obtained $Dq = 1510\ cm^{-1}$ and $B = 697\ cm^{-1}$. Three spin-allowed crystal field transitions are to be expected in optical spectra of octahedrally coordinated Cr^{3+} (octahedra M3 site, Fig. 34 in Deer et al. [1]) in the transition $^4A_2 \rightarrow {}^4T_2$ (^4F), band v_1, and also in the transition $^4A_2 \rightarrow {}^4T_1$ (^4F) band v_2. In the present case, band at 453 nm (22075 cm^{-1}) is the v_2 band and 658 nm band (15197 cm^{-1}) is the v_1 band, hence in our measurement, $B = 722\ cm^{-1}$. Since $v_1 = \Delta = 10\,Dq$, the value $Dq/B = 2.10$ is where one should look for the above transitions. The 691 nm band (14471 cm^{-1}) is due to the transition $^4A_{2g}$ (^4F) $\rightarrow {}^2T_1(^2G)$. Table 2 shows transitions, energy and wavelength for natural zoisite.

In many silicate minerals, usually one finds Fe^{2+}-band in the region of 900 to 1200 nm, for example Yauri et al. [33], Paião and Watanabe [34] and Souza et al. [35]. In our zoisite sample no Fe^{2+}-band has been observed, therefore, whole Fe contained in the sample is in 3^+-state. No transition in Fe^{3+} contributing to optical absorption spectrum has been observed, however Fe^{3+} ions do contribute significantly to EPR spectrum as we will see in sequence.

Cr^{3+} and Fe^{3+} in the EPR spectrum of zoisite

We consider the two sets of signals, called R1 and R2 in Fig. 2 unusual, in the sense that no similar case with such large signals is found in the literature. The shape and position of the two sets of lines suggests that Cr^{3+} and Fe^{3+} ions are in octahedral positions with a high degree of distortion. Intense gamma irradiation affects slightly the intensity of lines at low magnetic field. However it is interesting to note that with pre-annealing above 800 °C, high radiation dose (50 kGy) causes a decrease of the lines around $g = 3.72$ and $g = 4.13$.

On the other hand the six lines of Mn^{2+} centered at $g = 2$ and the broad EPR line of Fe^{3+} ion due to intense spin–spin interaction are superimposed. The experimental values of *g* and *A* are in agreement with those of Mn^{2+} in epidote minerals [21,23]. For heat treatment in 900 °C, it is noted that the signal around $g = 2.0$ grows significantly while signals R1 decrease indicating that the Fe^{3+} ions with signals in the vicinity of $g = 2$ increase at the expense of Fe^{3+} responsible for R2 signals. The results of XRD data (Fig. 1) indicate

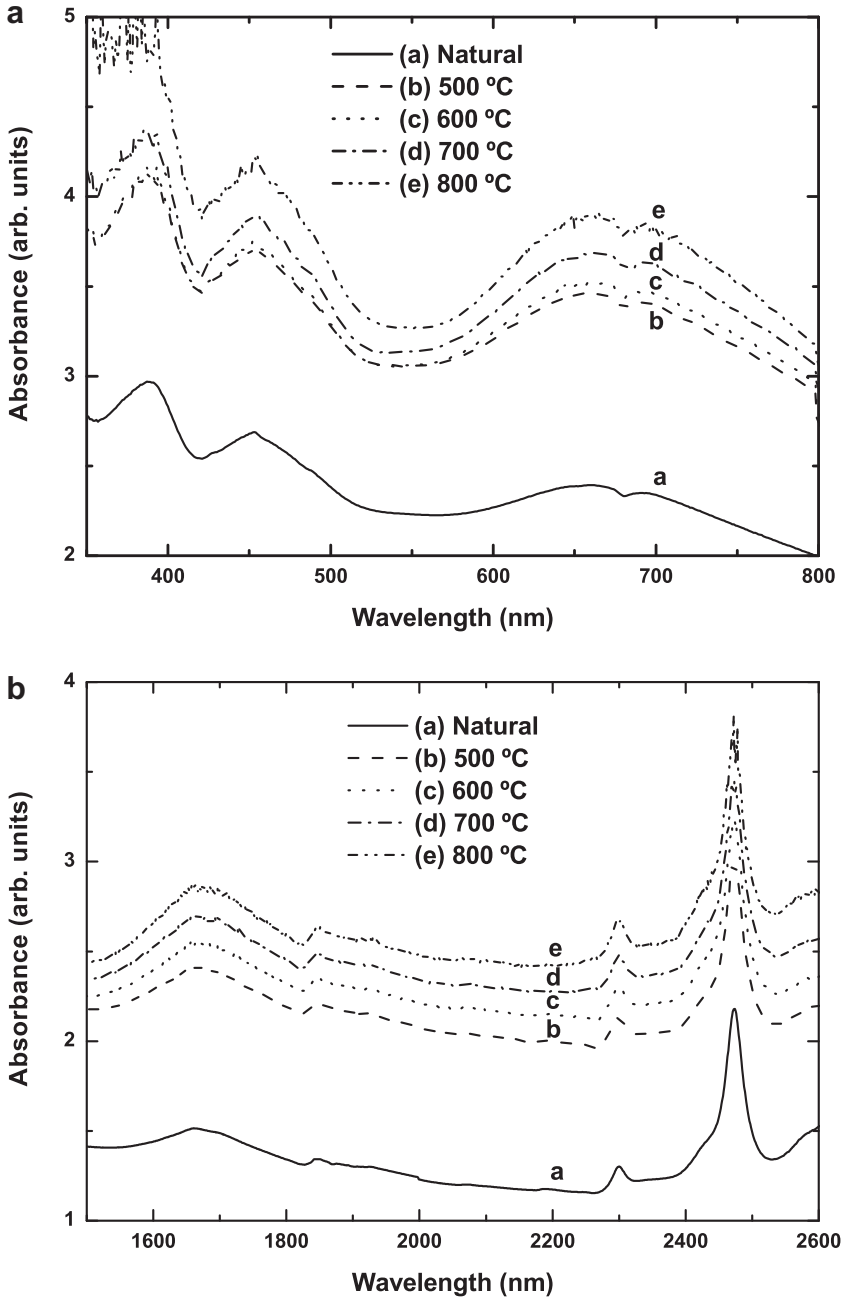

Fig. 5. Optical absorption of natural zoisite annealed at 500, 600, 700 and 800 °C. (a) Visible region and (b) infrared region. Heat treatments above 800 °C cause the breaking of the slabs used in the measurements.

that the crystal structure of zoisite resists to the severe heat treatment. Above 800 °C a rearrangement of Fe^{3+} and Mn^{2+} ions in tetrahedral and octahedral sites of the structure occurs. This rearrangement favors the proximity of iron ions with a strong tendency to form clusters.

Using the WinEPR program we have found the microwave absorption bands which in principle give rise to sets of lines between 500 and 2500 G. Eight absorption bands (Lorentzian-shaped) were fitted (Fig. 7) to EPR absorption spectrum and the calculated parameters of each are shown in Table 3.

Note that the deconvolution yields a band centered at $g = 4.3$ due to Fe^{3+} ion in an octahedral symmetry. In the EPR study in kaolinite mineral, Boesman and Schoemaker [36] observed the same shape and intensity of lines due to Fe^{3+} in a strong crystal field ($g = 2$ and $g_x = 3.52$, $g_y = 4.20$ and $g_z = 5.00$). On the other hand, works of Landry et al. [37] and Fournier et al. [38] in chromium glass silicates showed strong lines around $g = 5$ that increase with the amount of chromium in the structure. The signal at low field in our sample can be described by spin Hamiltonian:

$$H = g_0 \mu_B \vec{B} \cdot \vec{S} + D\left[S_z^2 - \frac{1}{3}S(S+1)\right] + E\left(S_x^2 - S_y^2\right) \quad (2)$$

where $g_0 = g_e - (g\lambda/\Delta)$, λ spin-orbit coupling constant, Δ is the separation between the ground and excited states, g_e is the free electron g value, μ_B is the Bohr magneton, $\vec{B}$ is the external magnetic-field intensity, $\vec{S}$ is the spin angular momentum operator. The terms D and E are axial (trihedral or tetrahedral) and orthorhombic crystal field parameters respectively. The parameter D

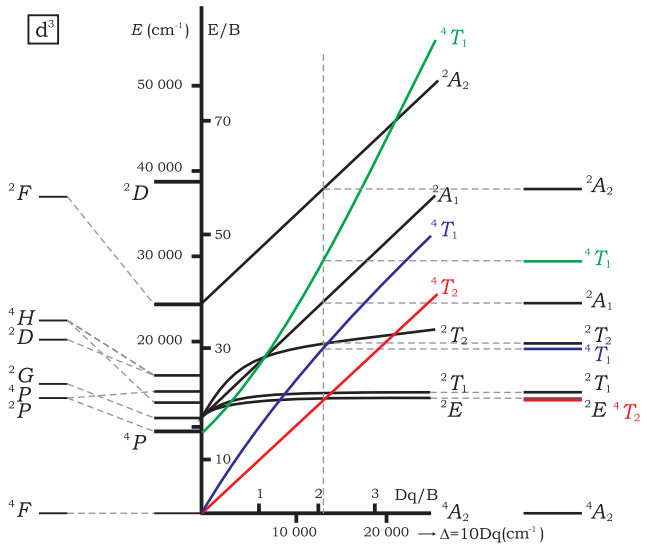

Fig. 6. Energy level diagram for Cr^{3+}, $3d^3$, in octahedral coordination calculated from spectral data for zoisite. Transitions are shown by the dashed line. The calculated values for the Racah parameters are: $B = 722\ cm^{-1}$, $C = 3367\ cm^{-1}$ and $Dq/B = 2.10$.

Table 2
Energy (ν) and wavelength (λ) of spin-allowed *dd* band of Cr^{3+} ion in OA spectra for zoisite. The positions of bands do not change with increase in annealing temperature.

λ (nm)	ν (cm^{-1})	Center/transition
427	23419	$[AlO_4/h]$
453	22075	$^4A_2 \rightarrow {}^4T_1$
658	15197	
662		$^4A_2 \rightarrow {}^4T_2$, $^4A_2 \rightarrow {}^2T_1$ (forbidden)
691	14471	

describes the splitting of the fundamental state, resulting in the Kramer doublets.

For the case $E = 0$ and $2|D| > h\nu$, where $h\nu$ is the energy of the microwave photon, the effect of the axial field on the $^4A_2$ term is then obtained by:

$$H' = D\left[S_z^2 - \frac{1}{3}S(S+1)\right] \tag{3}$$

The quartet is split into two doublets characterized by $m_S = \pm\frac{1}{2}$ and $m_S = \pm\frac{3}{2}$ and separated in energy by $2|D|$. In the presence of an external magnetic field ($E \neq 0$) the doublets split with energies:

$$E_{m_S=\pm\frac{1}{2}} = \pm\frac{1}{2}g\mu_B\left[B_z^2 + 4\left(B_x^2 + B_y^2\right)\right]^{\frac{1}{2}} \tag{4}$$

and

$$E_{m_S=\pm\frac{3}{2}} = \pm\frac{3}{2}g\mu_B B_z^2 \tag{5}$$

The low field peak near $g = 5.25$ then, barring unusually large individual line-widths, transitions within the $m_S = \pm\frac{1}{2}$ doublet are observed around $g = 2$ superimposed to Mn^{2+} and Fe^{3+} lines. On the other hand for $m_S = \pm\frac{3}{2}$ doublet, forbidden transitions are expected at $g = 3g_e$. But if the crystal field components of orthorhombic symmetry are present, the two sets of doublets become intermixed and the selection rule breaks down. Thus, it appears that the presence of a crystal field component of orthorhombic symmetry could result in the observed spectra.

An approximate upper bound on the zero-field splitting can also be obtained. Meijer and Gerritsen [39] have shown that the zero-field splitting 2D and $^4A_2$ level due to spin orbit coupling to higher levels in the presence of trigonal fields is given by:

$$2D = \frac{152}{9}\frac{\lambda^2\delta}{\Delta^2} \tag{6}$$

where δ is the difference in energy between the singlet and doublet split from $^4A_1$ level due to crystal field components of axial symmetry.

The most pronounced characteristic of the EPR spectrum in the zoisite sample is the intense line around $g = 2$. This feature can be accounted for if the spectrum is attributed to exchange coupled Cr^{3+} pairs using:

$$H = J\vec{S}_1 \cdot \vec{S}_2 + 2\mu_B B \cdot (\vec{S}_1 + \vec{S}_2) \tag{7}$$

$\vec{S}_1$ and $\vec{S}_2$ are interacting spins, J represents the isotropic portion of the exchange interaction. If the exchange term is assumed to dom-

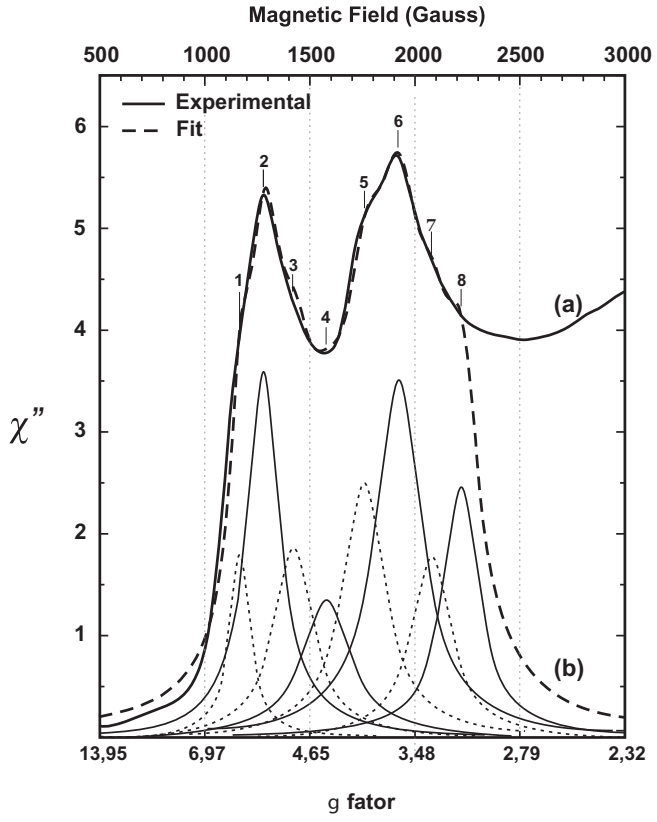

Fig. 7. (a) Microwave absorption bands obtained from R1 and R2 EPR spectra. (b) Deconvolution analysis of (a). The curve was fitted with eight absorption bands using the Bloch equations and the parameters are presented in Table 3.

Table 3
Graphic parameters of the absorption bands obtained of deconvolution spectrum. B_0 (G) is the central magnetic field, $\Delta B_{1/2}$ (G) is full width at half maximum, I (Arb. Units) is the Intensity and A (Arb. Units) is the area.

Ion	Peak	B_0 (G)	g	$\Delta B_{1/2}$ (G)	I (10^4)	A (10^6)
Cr^{3+}	1	1167.08	$g_x = 5.979$	120.91	1.79	2.17
	2	1279.18	$g_z = 5.455$	198.34	3.60	7.14
	3	1419.78	$g_y = 4.915$	230.49	1.87	4.31
Fe^{3+}	4	1578.52	$g_{\|\|} = 4.321$	284.00	1.35	3.83
Fe^{3+}	5	1761.00	$g_x = 3.963$	250.83	2.50	6.27
	6	1920.85	$g_z = 3.633$	270.07	3.50	9.46
	7	2080.13	$g_y = 3.355$	230.07	1.78	4.09
	8	2220.02	$g = 3.143$	210.54	2.46	5.17

inate Zeeman term and the line joining the two ions is taken as the z axis, then, the eigenvalues of Eq. (6) are given by:

$$E = \frac{1}{2}[JS\ (S+1) - S_1(S_1+1) - S_2(S_2+1)] + g_e\mu_B B m_S \quad (8)$$

For Cr^{3+}, $S_1 = S_2 = \frac{3}{2}$, and $S = 0, 1, 2, 3$. Since Cr_2O_3 exhibits antiferromagnetic properties [40], J is taken to be positive. In the case considered, no transitions can be induced between levels with different total spin S since J has been taken greater than the Zeeman splitting at resonance. The allowed $\Delta m_S = \pm 1$ transition within each S manifold all occur at $g = 2.0$. Therefore, the assumption of strong isotropic exchange coupling is adequate to account for the observed g-value in our sample.

Conclusions

The EPR spectrum of zoisite at room temperature show three intense set lines at $g \sim 6$, $g \sim 4$ and $g \sim 2$. Signals at 500–1500 G and 1500–2000 G was attributed to Cr^{3+} and Fe^{3+} ions respectively, both in octahedral positions under intense crystal field effects in axial direction.

On the other hand six lines of Mn^{2+} centered at $g = 2$ superimposes on the intense spin–spin interaction line due to Fe^{3+} ion. High temperature pre-annealing and 50 kGy gamma irradiation caused very small change in the shape and the intensity of lines for annealing temperatures below 800 °C. Using the deconvolution analysis eight absorption bands were fitted to EPR absorption spectrum. In particular the line centered at $g = 4.3$ due to Fe^{3+} ion in octahedral symmetry was identified as being similar to the line observed in other silicate minerals studied by different authors. Optical absorption spectrum shows several bands, the band at 427 nm is due to the aluminum center and the bands at 453, 658 and 691 nm were attributed to allowed transitions of Cr^{3+}. The sharp drop around 680 nm indicates the effect of a strong crystal field in the axial direction of the octahedral site which contains the Cr^{3+} ion. Other bands in the NIR region was attributed to vibrational modes of OH^-, OH and H_2O molecules in the crystal structure. OA spectra of annealed zoisite do not show changes in the bands except for an increase in the background absorption.

Acknowledgements

We would like to thank Ms. E. Somesari and Mr. C. Gaia for kindly carrying out irradiation of the samples. This work was supported by CAPES and FAPESP.

References

[1] W. Deer, R. Howie, J. Zussman, An Introduction to the Rock-Forming Minerals, second ed., Prentice Hall, 1996.
[2] W. Dollase, American Mineralogist 53 (1968) 1882–1898.
[3] G. Dorsam, A. Liebscher, B. Wunder, G. Franz, M. Gottschalk, American Mineralogist 92 (2007) 1133–1147.
[4] G. Franz, A. Liebscher, Reviews in Mineralogy and Geochemistry 56 (2004) 1–81.
[5] E. Gabe, J. Portheine, H. Simon, American Mineralogist 58 (1973) 218–223.
[6] C. Hurlbut Jr., American Mineralogist 54 (1969) 703–709.
[7] T. Ito, N. Morimoto, R. Sadanaga, Acta Crystallographica 7 (1954) 53–59.
[8] B. Angel, J. Jones, P. Hall, Clay Minerals 10 (1974) 247–255.
[9] H.J. Ccallata, L. Tomaz Filho, S. Watanabe, Spectrochimica Acta. Part A, Molecular and Biomolecular Spectroscopy 78 (2011) 1272–1277.
[10] M. Czaja, Z. Mazurak, M. Godlewski, A. Suchocki, Journal of Applied Spectroscopy 62 (1995) 643–647.
[11] G. Faye, E.H. Nickel, The Canadian Mineralogist 10 (1971) 812–821.
[12] D.R. Hutton, Journal of Physics C: Solid State Physics 4 (1971) 1251–1257.
[13] D.R. Hutton, G.J. Troup, G.A. Stewart, Science (New York, NY) 174 (1971) 1259.
[14] B. Koziarska, M. Godlewski, A. Suchocki, M. Czaja, Z. Mazurak, Physical Review B 50 (1994) 12297–12300.
[15] K. Langer, D. Lattard, American Mineralogist 65 (1980) 779–783.
[16] K. Langer, M. Raith, American Mineralogist 59 (1974) 1249–1258.
[17] K. Langer, E. Tillmanns, M. Kersten, H. Almen, R. Arni, Zeitschrift für Kristallographie 217 (2002) 563–580.
[18] A. Liebscher, M. Gottschalk, G. Franz, American Mineralogist 87 (2002) 909–921.
[19] B. Reddy, K. Sarma, Physica Academiae Scientiarum Hungaricas 52 (1982) 117–122.
[20] S.L. Reddy, K.S. Maheswaramma, R.R. Reddy, A.V. Reddy, Y. Nakamura, B. Reddy, T. Endo, R.L. Frost, Spectrochimica Acta. Part A, Molecular and biomolecular spectroscopy 78 (2011) 1240–1244.
[21] G. Srinivasulu, B. Sudhana, B. Reddy, R. Natarajan, P. Rao, Spectrochimica Acta. Part A: Molecular Spectroscopy 48 (1992) 1421–1425.
[22] M.N. Taran, K. Langer, European Journal of Mineralogy 12 (2000) 7–15.
[23] T. Tsang, S. Ghose, Journal of Chemical Physics 54 (1971) 856–862.
[24] B.W. Anderson, Journal of Gemmology 11 (1968) 1–6.
[25] S. Ghose, T. Tsang, Science (New York, NY) 171 (1971) 374–376.
[26] E. Malisa, Geology of the tanzanite gemstone deposits in the Lelatema area, NE Tanzania, Suomalainen Tiedeakatemia, 1987.
[27] V.K. Schmetzer, H.W. Berdesinski, Neves Jahrbuch Fur Mineralogie Monatshefte 5 (1978) 197–202.
[28] H.J. Ccallata, S. Watanabe, AIP Conference Proceedings 1265 (2010) 391–394.
[29] P. Game, Mineralogical Magazine 30 (1954) 458–466.
[30] M. Ikeya, New Applications of Electron Spin Resonance: Dating, Dosimetry and Microscopy, World Scientific Publishing Co. Pte. Ltd., Singapore River Edge, NJ, 1993.
[31] G.R. Hunt, J.W. Salisbury, C.J. Lenhoff, Modern Geology 4 (1973) 85–106.
[32] G. Fuxi, L. Huimin, Journal of Non-Crystalline Solids 80 (1986) 20–33.
[33] J. Yauri, N. Cano, S. Watanabe, Journal of Luminescence 128 (2008) 1731–1737.
[34] J. Paião, S. Watanabe, Physics and Chemistry of Minerals 35 (2008) 535–544.
[35] S. Souza, J. Chubaci, P.C. Selvin, M. Sastry, S. Watanabe, Journal of Physics D: Applied Physics 35 (2002) 1562–1565.
[36] E. Boesman, D. Schoemaker, Comptes Rendus Hebdomadaires des Séances de L'académie des Sciences 252 (1961) 1931–1933.
[37] R. Landry, J. Fournier, C. Young, Journal of Chemical Physics 46 (1967) 1285.
[38] J. Fournier, R. Landry, R. Bartram, Journal of Chemical Physics 55 (1971) 2522.
[39] P. Meijer, H. Gerritsen, Physical Review 100 (1955) 742.
[40] E. Trounson, D. Bleil, R. Wangsness, L. Maxwell, Physical Review 79 (1950) 542–543.